Green's function for photonic crystal slabs

Li-Ming Zhao, Xue-Hua Wang,* Ben-Yuan Gu,† and Guo-Zhen Yang
Institute of Physics, Chinese Academy of Sciences, P. O. Box 603, Beijing, China
(Received 1 February 2005; revised manuscript received 6 June 2005; published 31 August 2005)

Green's tensors for photonic crystal (PC) slabs are numerically solved by the coupled-dipole approximation (CDA) technique. The obtained components of Green's tensors satisfy discontinuous or continuous conditions at interfaces of scatterers. This shows that the CDA technique is very applicable to studying the properties of PC slabs. Green's tensors exhibit obviously periodic oscillation with the increase of the number of scatterers; furthermore, the effect of each scatterer on Green's tensors displays a localization feature in the sample containing one row of scatterers; on the contrary, this localized effect disappears in the sample consisting of multiple rows of scatterers.

DOI: 10.1103/PhysRevE.72.026614 PACS number(s): 42.70.Qs, 42.25.Fx, 42.25.Gy

I. INTRODUCTION

Recently, there has been great interest in photonic crystals (PCs), which possess periodic dielectric structures with the so-called photonic bandgaps (PBGs). PBGs can be used to effectively control the light propagation [1–6] and atomic spontaneous emission [7–10] in PCs. The three-dimensional (3D) PCs are favorable for some practical applications. However, it is still difficult to fabricate available 3D PCs served as photonic devices. An alternative system is the consideration of the PC slabs with two-dimensional (2D) periodicity and with the confinement in the third dimension by using the index contrast. PC slabs are not only easier to fabricate using existing techniques, but also they have the ability of realizing various controls of light waves. A number of experimental and theoretical studies on the PC slab structures have been reported [11–15]. It is believed that the PC slabs become preponderant for the miniaturization of individual optical devices, making the densely integrated photonic circuits possible.

The electromagnetic properties of infinite PC structures have been investigated extensively; however, real physical structures always are finite. It is expected that electromagnetic properties of finite PC structures may be significantly different from the infinite ones. The Green's tensor technique is especially useful for studying the electromagnetic properties of the finite PC structures. This technique has been shown to be greatly powerful in the calculations of light scattering, for instance, the surface scattering [16] and multilayer scattering [17,18]. On the other hand, the Green's tensor method has a great advantage in calculating the local density of states (LDOS) of photons [19–21], in particular, for the finite electromagnetic scattering systems. Recent studies have shown that the LDOS plays a very important role in determining quantum optical properties of atoms (molecules) in inhomogeneous electromagnetic environments [5,22,23]. A great deal of practice has demonstrated that the coupled-dipole approximation (CDA) can be applied to numerically solving the integral equation of the Green's tensors in scattering systems. Moreover, a powerful numerical method, in which the CDA is incorporated with the conjugated gradient algorithm and fast Fourier transform (CG-FFT), has been developed to solve the Green's tensors. This technique provides huge reductions in memory sizes and computing times [24–32]. The CDA with CGFFT has been successfully employed to calculate the Green's tensors of both 2D and 3D finite-size photonic crystals [21,24]. However, no existing studies on the Green's tensors of PC slabs have been reported so far.

Due to important applications of PC slabs to the optical devices, for instance, in the integrated photonic circuits, and microcavity laser, in this paper, we study the properties of the Green's tensors for the PC slabs by using the CDA with the CGFFT. The outline of this paper is as follows: Sec. II introduces the CDA technique used for calculating Green's tensors for PC slabs. The calculation results are presented in Sec. III, together with analysis. Finally, a brief summary is reserved in Sec. IV.

II. THE COUPLED-DIPOLE APPROXIMATION IN AN INTEGRAL EQUATION OF GREEN's TENSORS

Let us consider a scattering system consisting of a background with dielectric function $\epsilon^B(\mathbf{r})$ and some scatterers with the dielectric function $\epsilon^B(\mathbf{r})+\Delta\epsilon(\mathbf{r})$. When this system is illuminated by an incident electric field $\mathbf{E}^0(\mathbf{r})$, the total field $\mathbf{E}(\mathbf{r})$, and incident field $\mathbf{E}^0(\mathbf{r})$ satisfy the following vectorial wave equations, respectively;

$$\nabla \times \nabla \times \mathbf{E}(\mathbf{r}) - k_0^2[\epsilon^B(\mathbf{r}) + \Delta\epsilon(\mathbf{r})]\mathbf{E}(\mathbf{r}) = \mathbf{0}, \quad (1)$$

and

$$\nabla \times \nabla \times \mathbf{E}^0(\mathbf{r}) - k_0^2\epsilon^B(\mathbf{r})\mathbf{E}^0(\mathbf{r}) = \mathbf{0}, \quad (2)$$

where $k_0=\omega/c$ is the wave number in a vacuum. Equations (1) and (2) can be transformed as the following integral equations by the Green's tensors [24]:

$$\mathbf{E}(\mathbf{r}) = \mathbf{E}^0(\mathbf{r}) + \int_V d\mathbf{r}' \mathbf{G}^B(\mathbf{r},\mathbf{r}') \cdot k_0^2 \Delta\epsilon(\mathbf{r}')\mathbf{E}(\mathbf{r}'), \quad (3)$$

or

*Corresponding author. E-mail address: wangxh@aphy.iphy.ac.cn
†E-mail address: guby@aphy.iphy.ac.cn

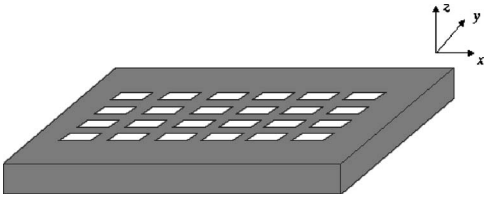

FIG. 1. Schematic of a two-dimensional square lattice PC slab consisting of rectangular holes etched on a finite thin slab, surrounded by air.

$$\mathbf{E}(\mathbf{r}) = \mathbf{E}^0(\mathbf{r}) + \int_V d\mathbf{r}' \mathbf{G}(\mathbf{r},\mathbf{r}') \cdot k_0^2 \Delta\epsilon(\mathbf{r}') \mathbf{E}^0(\mathbf{r}'), \quad (4)$$

where $\mathbf{G}(\mathbf{r},\mathbf{r}')$ and $\mathbf{G}^B(\mathbf{r},\mathbf{r}')$ are the corresponding Green's tensors to Eqs. (1) and (2), they satisfy the following equations:

$$\nabla \times \nabla \times \mathbf{G}(\mathbf{r},\mathbf{r}') - k_0^2[\epsilon^B(\mathbf{r}) + \Delta\epsilon(\mathbf{r})]\mathbf{G}(\mathbf{r},\mathbf{r}') = \mathbf{1}\delta(\mathbf{r}-\mathbf{r}') \quad (5)$$

and

$$\nabla \times \nabla \times \mathbf{G}^B(\mathbf{r},\mathbf{r}') - k_0^2 \epsilon^B(\mathbf{r}) \mathbf{G}^B(\mathbf{r},\mathbf{r}') = \mathbf{1}\delta(\mathbf{r}-\mathbf{r}'). \quad (6)$$

The Green's tensor $\mathbf{G}(\mathbf{r},\mathbf{r}')$ of the total scattering system and $\mathbf{G}^B(\mathbf{r},\mathbf{r}')$ of the background material fulfill Dyson's equation as

$$\mathbf{G}(\mathbf{r},\mathbf{r}') = \mathbf{G}^B(\mathbf{r},\mathbf{r}') + \int_V d\mathbf{r}'' \mathbf{G}^B(\mathbf{r},\mathbf{r}'') \cdot k_0^2 \Delta\epsilon(\mathbf{r}'') \mathbf{G}(\mathbf{r}'',\mathbf{r}'). \quad (7)$$

Evidently, the three column vectors of the Green's tensor $\mathbf{G}(\mathbf{r},\mathbf{r}')$ represent, respectively, the three electric fields at $\mathbf{r}$, radiated from three orthogonal unit dipoles at $\mathbf{r}'$.

Equation (7) can be well solved by using of the conventional coupled-dipole approximation (CDA) technique, that is, the scatterers are divided into N cells. We assume that the size of each cell is so small that the variations of the Green's tensors can be negligible within each individual cell and the cell location is assigned by its center of $\mathbf{r}_i$, and it has permittivity $\epsilon_i = \epsilon(\mathbf{r}_i)$ and volume ΔV_i. Equation (7) can then be discretized as algebraic equations

$$\mathbf{G}(\mathbf{r}_i,\mathbf{r}_0) = \mathbf{G}^B(\mathbf{r}_i,\mathbf{r}_0) + \sum_{k=1}^{N} \mathbf{G}^B(\mathbf{r}_i,\mathbf{r}_k) \cdot k_0^2 \Delta\epsilon(\mathbf{r}_k) \mathbf{G}(\mathbf{r}_k,\mathbf{r}_0) \Delta V_k, \quad (8)$$

where $\mathbf{r}_0$ denotes the position of the source point. We now decompose $\mathbf{G}(\mathbf{r}_i,\mathbf{r}_0) = \mathbf{G}^B(\mathbf{r}_i,\mathbf{r}_0) + \mathbf{G}^s(\mathbf{r}_i,\mathbf{r}_0)$, and $\mathbf{G}^s(\mathbf{r}_i,\mathbf{r}_0)$ is the scattering Green's tensor, which depends on the special properties of scatterers. Then Eq. (8) can be reformed as

$$\mathbf{G}^s(\mathbf{r}_i,\mathbf{r}_0) = \sum_{k=1}^{N} \mathbf{G}^B(\mathbf{r}_i,\mathbf{r}_k) \cdot k_0^2 \Delta\epsilon(\mathbf{r}_k) [\mathbf{G}^B(\mathbf{r}_k,\mathbf{r}_0) + \mathbf{G}^s(\mathbf{r}_k,\mathbf{r}_0)] \Delta V_k. \quad (9)$$

It is noted that $\mathbf{G}^B(\mathbf{r},\mathbf{r}')$ becomes divergent at $\mathbf{r}=\mathbf{r}'$ or when both $\mathbf{r}$ and $\mathbf{r}'$ are located inside the same scatterer volume V. This divergence can be overcome by an appropriate renormalization procedure, as described by Yaghjian in detail [32].

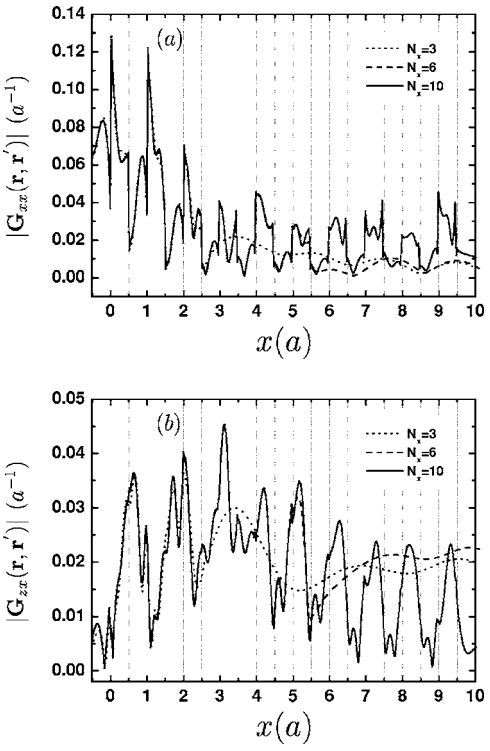

FIG. 2. Variations of the Green's tensors G_{xx} and G_{zx} with x for three different values of N_x=3, 6, and 10 when fixed N_y=1. The solid curve corresponds to N_x=10, the dashed curve to N_x=6, and the dotted curve to N_x=3. (a) for $G_{xx}(\mathbf{r},\mathbf{r}')$ and (b) for $G_{zx}(\mathbf{r},\mathbf{r}')$.

Equation (9) can be recast a set of a standard linear simultaneous equations as

$$\sum_{k=1}^{N} \mathbf{G}^B(\mathbf{r}_i,\mathbf{r}_k) \cdot k_0^2 \Delta\epsilon(\mathbf{r}_k) \mathbf{G}^B(\mathbf{r}_k,\mathbf{r}_0) = \sum_{k=1}^{N} [\delta_{i,k}\mathbf{1} - \mathbf{G}^B(\mathbf{r}_i,\mathbf{r}_k) \cdot k_0^2 \Delta\epsilon(\mathbf{r}_k) \Delta V_k] \mathbf{G}^s(\mathbf{r}_k,\mathbf{r}_0). \quad (10)$$

The Green's tensors within the scatterers can be obtained by solving the N linear simultaneous equations of Eq. (10). The conjugated gradient algorithm is used to solve these linear equations because it possesses the great advantage of saving memory. To save the computing times, the fast Fourier transform (FFT) technique has been employed [25–32]. In this paper, we focus on the examination of the characteristics of the Green's tensors of a PC slab. The background Green's tensor $\mathbf{G}^B(\mathbf{r},\mathbf{r}')$ is chosen as that of the stratified media [17,18]. It is worth pointing out that the Green's tensors in the stratified media no longer hold the same symmetry as those in an infinite homogenous background medium; therefore, it is impossible to apply the 3D FFT to expedite the computations. However, the 2D FFT can significantly speed

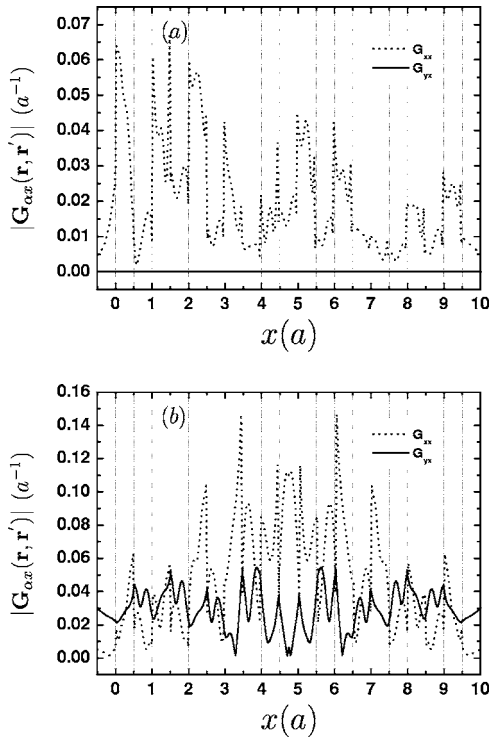

FIG. 3. Variations of the Green's tensors G_{xx} and G_{yx} with x for two different positions of the source point. The dotted curve stands for G_{xx} and solid curve for G_{yx}. (a) and (b) correspond to the source point at $(-1.0a, 0.25a, 0.25a)$ and $(4.75a, -3.0a, 0.25a)$, respectively.

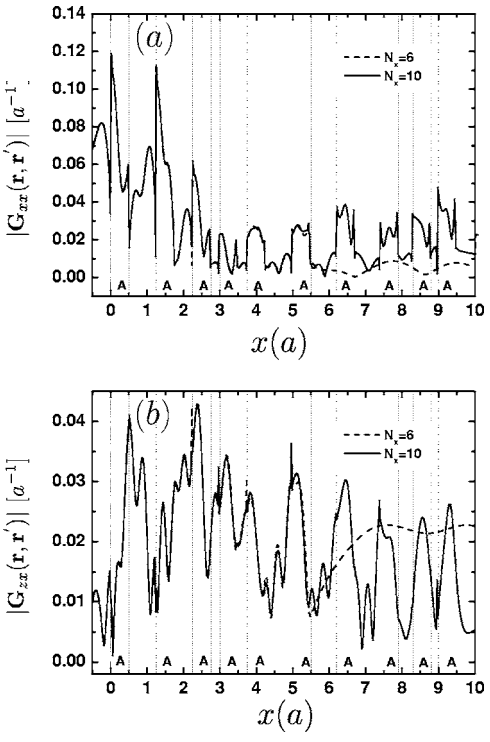

FIG. 4. Variations of the Green's tensors G_{xx} and G_{zx} with x for two different values of N_x=6 and 10 when fixed N_y=1. The arrangement of scatterers is aperiodic and the scattered regions are denoted by the symbol "A". The solid curve corresponds to N_x =10, and the dashed curve to N_x=6. (a) for $G_{xx}(\mathbf{r},\mathbf{r}')$ and (b) for $G_{zx}(\mathbf{r},\mathbf{r}')$.

the computations due to the existence of the symmetry of the tensor in the xy plane.

To apply the FFT in the x and y directions, we mathematically extend the scattered region in the xy plane into a rectangular block, double the lattice size in the x and y directions, and we consider the periodicity of the corresponding physical quantity [31]. In order to clarify this problem in brief, we reform Eq. (10) as

$$Y_i = \sum_{k_z=1}^{N_z} \sum_{k_y=1}^{2N_y} \sum_{k_x=1}^{2N_x} A_{ik} X_k, \tag{11}$$

where $Y_i = \Sigma_{k=1}^{N} \mathbf{G}^B(\mathbf{r}_i,\mathbf{r}_k)\cdot k_0^2 \Delta\epsilon(\mathbf{r}_k)\mathbf{G}^B(\mathbf{r}_k,\mathbf{r}_0)$, $A_{ik} = [\delta_{i,k}\mathbf{1} - \mathbf{G}^B(\mathbf{r}_i,\mathbf{r}_k)\cdot k_0^2\Delta\epsilon(\mathbf{r}_k)\Delta V_k]$, $X_k = \mathbf{G}^s(\mathbf{r}_k,\mathbf{r}_0)$, and $N = N_x N_y N_z$ is the total number of the discretized lattice sites. It is clearly seen that the elements of A_{ik} are dependent only on the displacment vector $\mathbf{p}_{ik} = \mathbf{p}_i - \mathbf{p}_k$, where $\mathbf{p}_i = (x_i, y_i)$; thus, Eq. (11) now can be written in a convolution form:

$$Y_i = \sum_{k_z=1}^{N_z} \sum_{k_y=1}^{2N_y} \sum_{k_x=1}^{2N_x} A'_{i-k} X_k. \tag{12}$$

As Eq. (12) possesses a convolution form, and if we perform the Fourier transform in the x and y directions, keeping the z dependency in the orginal domain, we then obtain the following summation in the z direction:

$$\hat{Y}_{n_x,n_y,i_z} = \sum_{k_z=1}^{N_z} \hat{A}'_{n_x,n_y,i_z-k_z} \hat{X}_{n_x,n_y,k_z}, \tag{13}$$

where the caret symbol denotes the Fourier transform. The 2D-FFT technique has been discussed in detail in Ref. [26] and testified to be an effective method for speeding the computations.

The iteration process of solving Eq. (12) based upon the conjugated-gradient algorithm and 2D FFT is briefly described as follows: First, we give an initial guess X_k^t for the column vector X_k and calculate its Fourier transform. Then we calculate the $\hat{Y}^t_{n_x,n_y,i_z}$ by Eq. (13) and $Y^t_{n_x,n_y,i_z}$ by the inverse 2D FFT. Afterward, we compare Y^t with Y and generate the new X_k^t by the conjugated-gradient algorithm. This process is repeated until the obtained solution satisfies the desirable convergency accuracy. This method approximately requires total memories of $\sim 4NN_z$ and the CPU operations of $\sim 4L_i N N_z$ (here L_i denotes the iteration times), much less than N^2. Therefore, this method can be applied to treat the scattering problems of the large size structures.

III. RESULTS AND ANALYSIS

The model structure considered is sketched in Fig. 1. The PC slab consists of rectangular holes etched on a finite-scaled thin slab surrounded by air. The dielectric constant of the thin slab sets ϵ_s=3. We assume that the central distance

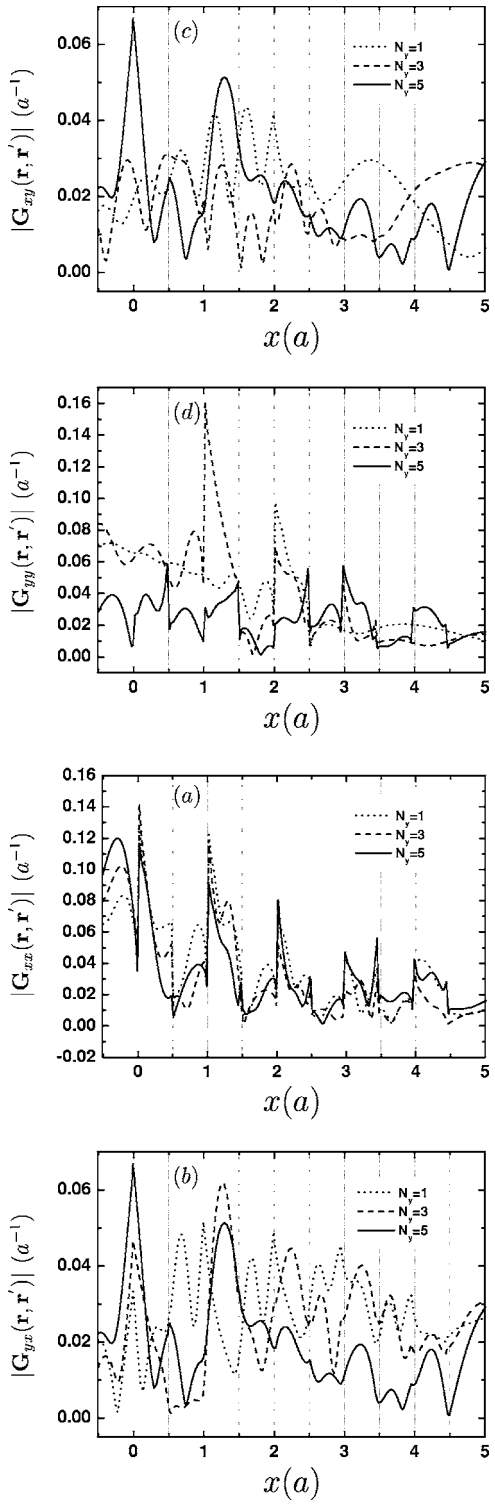

FIG. 5. Variations of the Green's tensors G_{xx} or G_{xy} and G_{yx} or G_{yy} with x or y for N_x=5 and N_y=1, 3, and 5. The dotted curve corresponds to the Green's tensors for N_y=5, the dashed curve to N_y=3, and the dotted curve to N_y=1. (a) for $G_{xx}(\mathbf{r},\mathbf{r}')$, (b) for $G_{yx}(\mathbf{r},\mathbf{r}')$, (c) for $G_{xy}(\mathbf{r},\mathbf{r}')$, and (d) for $G_{yy}(\mathbf{r},\mathbf{r}')$.

of the nearest hole-to-hole is a, both the length and width of each hole are the same as $0.5a$, and the thickness of the slab is chosen to be $0.5a$. The number of holes along the x or y direction is selected by N_x or N_y. In the following calculations, the wavelength of the incident light is $\lambda=1.0a$ and the discretized step is $dx=dy=\lambda/26$. This implies that a unit cell is discretized into 8788 lattice sites.

We first study the Green's tensors for the structure shown in Fig. 1. To reveal the influence of the number of scatterers on the Green's tensors, we begin with the case of one row of scatterers, i.e., $N_y=1$. For brevity, we choose the coordinate origin at the left lower corner of the first scatterer, i.e., $\mathbf{r}_0=(x_0,y_0,z_0)=(0,0,0)$. The qth scatterer occupies the region of $(q-1)a\leqslant x\leqslant(q-\frac{1}{2})a$, $0\leqslant y\leqslant 0.5a$, and $0\leqslant z\leqslant 0.5a$. The spacial variations of two components of Green's tensors $G(\mathbf{r},\mathbf{r}')$ along the x axis are displayed in Fig. 2: (a) for $G_{xx}(\mathbf{r},\mathbf{r}')$ and (b) for $G_{zx}(\mathbf{r},\mathbf{r}')$. The solid curve corresponds to the case of $N_x=10$, the dashed curve to $N_x=6$, and the dotted curve to $N_x=3$. The source point is placed at $\mathbf{r}'=(-1.0a,-3.0a,0.25a)$ and the observation line is chosen as $\mathbf{r}=(x,0.25a,0.4a)$. It is clearly seen that the change of the number of scatterers can significantly modify the Green's tensors. As the number of scatterers increases, the Green's tensor exhibits striking oscillations. We also observe the interesting behavior that when the number of scatterers is increased to 6, no significant change in the Green's tensor is observed in the region of $x<2.5a$, while the Green's tensors exhibit remarkable changes in the regions occupied by new additional scatterers. Similarly, so does the behavior in the case of $N_x=10$. This concludes that the influence of scatterers on the Green's tensors exhibits the localized feature. Furthermore, it is evident that the variations G_{zx} as a function of x are continuous at every interface of the individual scatterer, marked by the dotted vertical line. In contrast, G_{xx} is discontinuous, and the values of Green's tensors at the interfaces toward the scatterer sides are larger than those at the interface toward the background. From a physical viewpoint, $G_{xx}(\mathbf{r},\mathbf{r}')$ and $G_{zx}(\mathbf{r},\mathbf{r}')$, respectively, correspond to the x and z components of the electric fields, radiated from a unit electric dipole with the polarization parallel to the x axis. Therefore, it is apparent that the tangential component of the electric fields should be continuous across all interfaces, while their normal component should jump at the interfaces. These results are apparently associated with the continuity of the electric displacement and discontinuity of the dielectric constant. The dielectric constant of the scatterers is smaller than that of the background medium; therefore, G_{xx} in the scatterers should be larger than that in the background medium at the vicinity of the interfaces. Finally, it is interesting to note that in the case of $N_x=10$, the Green's tensors approximately exhibits periodic oscillatory behavior in the region far from the source point. It is reasonably concluded that the oscillations exhibit perfect periodicity when $N_x\gg 10$.

We now examine the characteristics of the Green's tensor for two different source points located at $\mathbf{r}'=(-1.0a,0.25a,0.25a)$ and $\mathbf{r}'=(4.75a,-3.0a,0.25a)$, respectively. The variations of G_{xx} and G_{yx} as a function of x in the case of $N_x=10$ are demonstrated in Figs. 3(a) and 3(b) for two different source points. The other parameters remain unchanged, and are the same as those in Fig. 2. The dotted curve corresponds to the variations of Green's tensor G_{xx} with x and solid curve to G_{yx}. A similar characteristic, for

instance, the discontinuity of the normal component of the Green's tensor at the interfaces, can be observed once again. We have also performed the numerical calculations in the cases of $N_x=3$ and 6 and the localized phenomenon of the Green's tensor at the scatterers is also observed. It is worth emphasizing an interesting result that $G_{yx}=0$ in Fig. 3(a). This arises from $G^B_{yx}=0$ when $y=y'$ for the stratified structures, where y and y' denote the positions of the observation and source points along the y axis, respectively. As mentioned above, $G^B_{\alpha,x}$ can be regarded as an incident field, excited by a unit electric dipole with a polarization orientation parallel to the x axis and propagating in the background of the stratified structures. Therefore, $G_{\alpha,x}$ is generated from the scattering of this incident field by the scatterers. $G^B_{yx}=0$ means that the incident field does not have a nonzero y component. As the interfaces of each scatterer are planar, a new component, i.e., the y component of the scattering field, can never be generated. Consequently, $G_{yx}=0$ is always held. In Fig. 3(b), it is evident that the Green's tensors exhibit a symmetric profile, which is attributed to the symmetry of the model structure along the x axis with respect to the source point.

The characteristics of the Green's tensors in the aperiodic arranging scatterers are shown in Fig. 4, in which the scattered regions are marked by the symbol "A". The other parameters are chosen as the same as those in Fig. 2. Comparing this plot with Fig. 2, it is found that some characteristics still are held, for instance, the oscillation behavior, the localized feature of the Green's tensors, and the continuous or discontinuous properties of the Green's tensors at the interfaces. However, the pattern of the oscillations and the oscillatory amplitude are significantly changed when the arrangement of the scatterers are modified.

We now turn to investigate the Green's tensors in a 2D PC slab. We select $N_x=5$, $N_y=1$, 3, and 5. The scatterers are labeled by the two indices $q(q_1,q_2)$ and the qth scatterer occupies the region as

$$\begin{cases} (q_1-1)a \leqslant x \leqslant (q_1-0.5)a, \\ [q_2-(N_y-3)/2]a \leqslant y \leqslant [q_2-(N_y/2-2)]a, \\ 0 \leqslant z \leqslant 0.5a, \end{cases}$$

where $N_y=1$, 3, and 5; $1 \leqslant q_1 \leqslant N_x$ and $1 \leqslant q_2 \leqslant N_y$. The source point is located at $\mathbf{r}'=(-1.0a,-1.0a,0.25a)$ and the observation line is denoted by $\mathbf{r}=(x,2.25a,0.4a)$ in Figs. 5(a) and 5(b) and $\mathbf{r}=(2.25a,y,0.4a)$ in Figs. 5(c) and 5(d). The solid curve corresponds to the Green's tensors in the case of $N_y=5$, the dashed curve to $N_y=3$, and the dotted curve to $N_y=1$. The discontinuity of G_{xx} or G_{yy} at every interface usually appears. However, the Green tensors are greatly sensitive to the change of N_y. This implies that the influence of scatterers in the 2D PC slab on the Green's tensors no longer exhibits any localized feature. It is worth pointing out that although only the components of G_{xx}, G_{yx}, and G_{zx} are depicted above, it is believed that the obtained results should be valid for other components of the Green's tensors.

IV. SUMMARY

The variations of Green's tensors with the number of scatterers are examined by using the CDA technique with CG-FFT. The numerical results show that the Green's tensors meet well the physical requirements at interfaces. This infers that the CDA technique can be successfully applied to the studies of the properties of the PC slabs. The Green's tensors exhibit striking oscillations as the number of scatterers increases; furthermore, the effect of each scatterer on the Green's tensors proves to be local for the sample only with one row of scatterers; on the contrary, this localized effect disappears for the sample consisting of multiple rows of scatterers.

ACKNOWLEDGMENTS

This work was supported by the Chinese National Key Basic Research Special Fund, Grant No. 2001CB610402.

[1] E. Yablonovitch, Phys. Rev. Lett. **58**, 2059 (1987); S. John, Phys. Rev. Lett. **58**, 2486 (1987).
[2] K. M. Ho, C. T. Chan, and C. M. Soukoulis, Phys. Rev. Lett. **65**, 3152 (1990).
[3] E. Yablonovitch, T. J. Gmitter, and K. M. Leung, Phys. Rev. Lett. **67**, 2295 (1991).
[4] A. Mekis, J. C. Chen, I. Kurland, S. Fan, P. R. Villeneuve, and J. D. Joannopoulos, Phys. Rev. Lett. **77**, 3787 (1996).
[5] X. H. Wang, B. Y. Gu, Z. Y. Li, and G. Z. Yang, Phys. Rev. B **60**, 11417 (1999); R. Wang, X. H. Wang, B. Y. Gu, and G. Z. Yang, J. Appl. Phys. **90**, 4307 (2001); Y. S. Zhou, B. Y. Gu, and F. H.Wang, J. Phys.: Condens. Matter **15**, 4109 (2003).
[6] M. Straub, M. Ventura, and M. Gu, Phys. Rev. Lett. **91**, 043901 (2003).
[7] S. John and J. Wang, Phys. Rev. Lett. **64**, 2418 (1990); Phys. Rev. B **43**, 12772 (1991); S. John and T. Quang, Phys. Rev. Lett. **74**, 3419 (1995); S. John and T. Quang, *ibid.* **76**, 1320 (1996).
[8] S. Bay, P. Lambropoulos, and K. Molmer, Phys. Rev. Lett. **79**, 2654 (1997); Phys. Rev. A **55**, 1485 (1997).
[9] J. Martorell and N. M. Lawandy, Phys. Rev. Lett. **65**, 1877 (1990); E. P. Petrov, V. N. Bogomolov, I. I. Kalosha, and S. V. Gaponenko, Phys. Rev. Lett. **81**, 77 (1998); M. Megens, J. E. G. J. Wijnhoven, A. Lagendijk, and W. L. Vos, Phys. Rev. A **59**, 4727 (1999).
[10] X. H. Wang, R. Wang, B. Y. Gu, and G. Z. Yang, Phys. Rev. Lett. **88**, 093902 (2002); X. H. Wang, B. Y. Gu, R. Wang, and H. Q. Xu, Phys. Rev. Lett. **91**, 113904 (2003); X. H. Wang, Y. S. Kivshar, and B. Y. Gu, Phys. Rev. Lett. **93**, 073901 (2004).
[11] R. D. Meade, A. Devenyi, J. D. Joannopoulos, O. L. Alerhand, D. A. Smith, and K. Kash, J. Appl. Phys. **75**, 4753 (1994); P. L. Gourley, J. R. Wendt, G. A. Vawter, T. M. Brennan, and B. E. Hammons, Appl. Phys. Lett. **64**, 687 (1994).
[12] R. Coccioli, M. Boroditsky, K. W. Kim, Y. Rahmat-Sammi,

and E. Yablonovitch, IEE Proc.: Optoelectron. **145**, 391 (1998); S. G. Tikhodeev, A. L. Yablonskii, E. A. Muljarov, N. A. Gippius, and T. Ishihara, Phys. Rev. B **66**, 045102 (2002).
[13] S. G. Johnson, S. Ian, P. R. Villeneuve, J. D. Joannopoulos, and L. A. Kolodziejski, Phys. Rev. B **60**, 5751 (1999); E. Chow, S. Y. Lin, S. G. Johnson, P. R. Villeneuve, J. D. Joannopoulos, J. R. Wendt, G. A. Vawter, W. Zubrzycki, H. Hou, and A. Alleman, Nature (London) **407**, 983 (2000).
[14] S. Noda, A. Chutinan, and M. Imada, Nature (London) **407**, 608 (2000).
[15] M. Kafesaki, M. Agio, and C. M. Soukoulis, J. Opt. Soc. Am. B **19**, 2232 (2002).
[16] J. E. Sipe, J. Opt. Soc. Am. B **4**, 481 (1987).
[17] M. S. Tomaš, Phys. Rev. A **51**, 2545 (1995).
[18] M. Paulus, P. Gay-Balmaz, and O. J. F. Martin, Phys. Rev. E **62**, 5797 (2000).
[19] A. A. Asatryan, K. Busch, R. C. McPhedran, L. C. Botten, C. M. deSterke, and N. A. Nicorovici, Phys. Rev. E **63**, 046612 (2001).
[20] R. C. McPhedran, L. C. Botten, J. McOrist, A. A. Asatryan, C. M. deSterke, and N. A. Nicorovici, Phys. Rev. E **69**, 016609 (2004).
[21] O. J. F. Martin, C. Girard, D. R. Smith, and S. Schultz, Phys. Rev. Lett. **82**, 315 (1999).
[22] R. Sprik, B. A. Van Tiggelen, and A. Lagendijk, Europhys. Lett. **35**, 265 (1996).
[23] R. Wang, X. H. Wang, B. Y. Gu, and G. Z. Yang, Phys. Rev. B **67**, 155114 (2003).
[24] O. J. F. Martin and N. B. Piller, Phys. Rev. E **58**, 3909 (1998).
[25] P. J. Flatau, Opt. Lett. **15**, 1205 (1997).
[26] R. Schmehl, B. M. Nebeker, and E. D. Hirleman, J. Opt. Soc. Am. A **14**, 3026 (1997).
[27] O. J. F. Martin, C. Girard, and A. Dereux, Phys. Rev. Lett. **74**, 526 (1995).
[28] O. J. F. Martin, A. Dereux, and C. Girard, J. Opt. Soc. Am. A **11**, 1073 (1994).
[29] B. T. Draine and P. J. Flatau, J. Opt. Soc. Am. A **11**, 1491 (1994).
[30] C. T. Tai, *Dyadic Green Function in Electromagnetic Theory* (IEEE Press, Piscataway, NJ, 1994).
[31] J. J. Goodman, B. T. Draine, and P. J. Flatau, Opt. Lett. **16**, 1198 (1991).
[32] A. K. Yaghjian, Proc. IEEE **68**, 248 (1980).